A particle-level rigid fiber model for high-Reynolds number flow, implemented in a general-purpose CFD code

Jelena Andric[1], Stefan B. Lindström[2], Srdjan Sasic[1] and Håkan Nilsson[1]

[1] Department of Applied Mechanics, Chalmers University of Technology, 412 96 Göteborg, Sweden
[2] Department of Management and Engineering, The Institute of Technology, Linköping University, 581 83 Linköping, Sweden

Keywords: rigid fiber model, particle level simulation, open-source CFD

Abstract

A particle-level rigid fiber model has been integrated into a general-purpose, open source computational fluid dynamics code to carry out detailed studies of fiber–flow interactions in realistic flow fields. The fibers are modeled as chains of cylindrical segments, and their translational and rotational degrees of freedom are considered. The equations of motion contain the contributions from hydrodynamic forces and torques, and the segment inertia is taken into account. The model is validated for the rotational motion of isolated fibers in simple shear flow, and the computed period of rotation is in good agreement with the one computed using Jeffery's equation for a prolate spheroid with an equivalent aspect ratio. The model is applied by suspending a number of fibers in the swirling flow of a conical diffuser, resembling one stage in the dry-forming of pulp mats. The Reynolds-averaged Navier–Stokes equations with an eddy-viscosity turbulence model are employed to describe the fluid motion, and a one-way coupling between the fibers and the fluid phase is included. The dependence of the fiber motion on initial position and density is analyzed.

Introduction

The dynamics of fiber suspensions are of great interest and importance in many industrial processes. The suspensions of fibers and fiber flocs are processed to produce paper products and fiber composites. One example is the making of wood fiber mats for use in hygiene products. The orientation and spatial distribution of fibers affect the macroscopic properties of the produced material, such as elastic modulus, strength, and thermal and electric conductivities. In pulp and paper processing, the fiber dynamics of the sheet forming process are one of the most important factors that influence the sheet characteristics (Ross and Klingenberg 1997; Matsuoka and Yamamoto 1995).

To model wet forming of paper and dry forming of pulp mats, it is necessary to consider large particle systems in high Reynolds number flow with finite Reynolds number fiber–flow interactions (Lindström 2008). Water-based papermaking has been previously modeled at particle-level with flexible fibers and direct numerical simulation (DNS) under a Stokes flow assumption (Svenning et al. 2012) and with a microhydrodynamics approach for finite Reynolds numbers (Lindström and Uesaka 2008; Lindström et al. 2009). Dry forming is even more numerically challenging, with large flow geometries and fibers suspended in air that is less dissipative than water. The aim of this paper is to describe a method suitable for handling such flows, and apply it to the fiber motion in the swirling flow in a conical diffuser.

Several numerical approaches have been developed to study particle-laden flows. In the Eulerian–Eulerian approach the phases are treated as interpenetrating continua. The Lagrangian–Eulerian approach, on the other hand, treats particles as moving objects in a fluid medium. In the DNS approach, the particle geometries are resolved to a high level of detail, giving excellent predictive capability for fiber motion in suspension (Qi 2006; Salahuddin et al. 2012), but at a high computational cost. In the microhydrodynamics approach, many particles are combined into multi-rigid-body systems, significantly reducing the computational cost. The choice of model is always a trade-off between accuracy and system size, as previously discussed by Crowe et al. (1998), Lindström and Uesaka (2007) and Hämäläinen et al. (2011).

Several variants of the microhydrodynamics approach have been previously developed to simulate flexible fiber motion in shear and sedimentation flows. Matsuoka and Yamamoto (1995) developed a particle-level simulation technique to capture the dynamics of rigid and flexible fibers in a prescribed flow field. They represented a fiber by a set of spheres, lined up and connected to each neighboring sphere. Ross and Klingenberg (1997) proposed a similar model, but using a chain of rigid, prolate spheroids. These numerical studies were in qualitative agreement with experimental results for isolated fiber motion obtained by Forgacs and Mason (1959a,b) and also predicted some of the rheological properties of fiber suspensions. Schmid et al. (2000) developed a particle-level simulation technique to study flocculation of fibers in sheared suspensions in three dimensions. They investigated the influence of the shear rate, fiber shape, fiber flexibility, and frictional inter-particle forces on flocculation. The fibers were modeled as chains of massless, rigid cylinder segments interacting with an imposed flow field through viscous drag forces and with

other fibers through contact forces. Lindström and Uesaka (2007) further developed the model of Schmid *et al.* (2000), by taking into account the particle inertia and the intermediate to long-range hydrodynamic interactions between the fibers.

In the present work, a rigid particle-level fiber model is implemented in the OpenFOAM, open source computational fluid dynamics (CFD) software (Weller *et al.* 1998). For fibers suspended in air, the hydrodynamic interactions are too weak to bend the fiber, so that the fibers can be treated as rigid bodies in their interaction with the flow. Therefore, the microhydrodynamics model with flexible fibers proposed by Lindström and Uesaka (2007) can be simplified by taking the fibers to be rigid. (Small deformations can however still be important when fiber interlock to form flocks, but that is beyond the scope of the present investigation). This is extremely beneficial for the time-efficiency of the implementation. The implemented model is validated against the known result for Jeffery's orbits for the rotational motion of an isolated fiber in low segment Reynolds number shear flow. The fiber model is applied to the motion of a number of cylindrical rigid fibers in the swirling high Reynolds number flow in a conical diffuser, reminiscent of a unit step in the dry-forming process. The fiber reorientation is studied, as determined by the fiber's initial position, length and density.

Nomenclature

Roman symbols

d	diameter (m)
l	length (m)
m	mass (kg)
$\vec{r}$	position (m)
$\dot{\vec{r}}$	velocity (ms^{-1})
$\ddot{\vec{r}}$	acceleration (ms^{-2})
$\hat{z}$	orientation vector ($-$)
$\overline{\overline{I}}$	inertia tensor (kgm^2)
$\dot{\overline{\overline{I}}}$	inertia tensor time derivative (kgm^{2}s^{-1})
$\vec{F}$	force (N)
$\vec{T}$	torque (Nm)
$\overline{\overline{A}}$	resistance tensor (kgs^{-1})
$\overline{\overline{C}}$	resistance tensor (kgs^{-1})
$\overline{\overline{E}}$	strain rate tensor (s^{-1})
$\overline{\overline{H}}$	resistance tensor (kgs^{-1})
C_D	drag coefficient ($-$)
Re	Reynolds number ($-$)
T	oscillatory period (s)
Δt	time step (s)
t	time (s)
k	kinetic energy (kgm^{2}s^{-2})
I	turbulent intensity($-$)
U	axial velocity component (ms^{-1})
W	tangential velocity component (ms^{-1})

Greek symbols

ρ	density (kgm^{-3})
ν	kinematic viscosity (m^{2}s^{-1})
η	dynamic viscosity(kgm^{-1}s^{-1})
$\dot{\gamma}$	shear rate (s^{-1})
$\overline{\overline{\delta}}$	Kronecker delta symbol (-)
$\vec{\omega}$	angular velocity (s^{-1})
$\vec{\upsilon}$	fluid velocity (ms^{-1})
$\vec{\Omega}$	angular velocity (s^{-1})
$\vec{\psi}$	random vector
ε	dissipation (m^{2}s^{-3})
τ	relaxation time (s^{-1})

Subscripts

i	segment index
n	time step index
s	segment
G	fiber's center of mass

Superscripts

h	hydrodynamic
υ	viscous
I	dynamic
ω	body
e	eddy
t	turbulent
tr	transit
$fluct$	fluctuating

Fiber Model

First, the fiber geometry and the governing equations for the fiber motion are described, followed by approximations for hydrodynamic forces and torques. The discretized governing equations are also presented.

Fiber Geometry. A fiber is modeled as a chain of N rigid cylindrical segments (Schmid *et al.* 2000; Lindström and Uesaka 2007), see Fig. 1. The segments are indexed $i \in 1, N$ and their locations are specified with respect to a global Cartesian coordinate system Γ. The axes of this inertial frame are defined by the base vectors $\{\hat{e}_1, \hat{e}_2, \hat{e}_3\}$ and the origin is denoted by O. A single fiber segment has a diameter d_i, a length l_i, a start point P_i, and a unit vector $\hat{z}_i$, which is aligned with the segment. The position of each fiber segment's center of mass is thus $\vec{r}_i = \overrightarrow{OP_i} + l_i\hat{z}_i/2$. The center of mass of the fiber is then defined as

$$\vec{r}_G = \frac{\sum_i m_i \vec{r}_i}{m} \tag{1}$$

where m_i is the mass of segment i and $m = \sum_i m_i$ is

the fiber mass. A fiber translates and rotates around its center of mass, while the relative angle between the orientation vectors of two adjacent fiber segments remains constant, *i.e.* a fiber cannot deform.
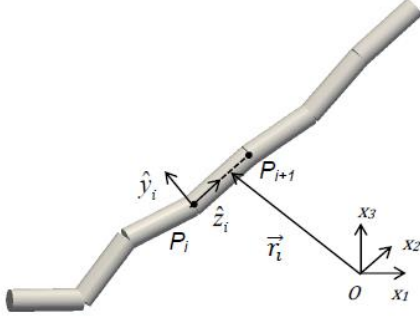

Figure 1: Fiber geometry definitions

Equations of Motion.

The linear momentum equation reads

$$m_i \ddot{\vec{r}}_G = \sum_i \{ \vec{F}_i^h + \vec{F}_i^w \} \tag{2}$$

where $\vec{F}_i^h$ is the hydrodynamic force acting on segment i and $\vec{F}_i^w$ is the sum of body forces. In the present work, $\vec{F}_i^w = m_i \vec{g}$, where $\vec{g}$ is the gravitational acceleration vector.

The angular momentum equation reads

$$\bar{\bar{I}}_G \cdot \dot{\vec{\omega}} + \vec{\omega} \times (\bar{\bar{I}}_G \cdot \vec{\omega}) = \sum_i \{ \vec{T}_i^h + \vec{r}_{Gi} \times (\vec{F}_i^h + \vec{F}_i^w) \}, \tag{3}$$

where $\vec{\omega}$ is the fiber angular velocity, $\bar{\bar{I}}_G$ is the fiber inertia tensor with respect to its center of mass and the global frame of reference, and $\vec{T}_i^h$ is the hydrodynamic torque on segment i. The inertia tensor for fiber segment i with respect to $\vec{r}_i$ is

$$\bar{\bar{I}}_i = \frac{1}{8} m_i d_i^2 \hat{z}_i \hat{z}_i^T + (\frac{1}{16} m_i d_i^2 + \frac{1}{12} m_i l_i^2)(\bar{\bar{\delta}} - \hat{z}_i \hat{z}_i^T). \tag{4}$$

Using the parallel axis theorem, the tensor of inertia for segment i with respect to the fiber center of mass is

$$\bar{\bar{I}}_{Gi} = \bar{\bar{I}}_i + m_i \left[(\vec{r}_{Gi} \cdot \vec{r}_{Gi}) \delta - \vec{r}_{Gi} \vec{r}_{Gi}^T \right], \tag{5}$$

with $\vec{r}_{Gi} = \vec{r}_i - \vec{r}_G$. The inertia tensor of the whole fiber is

then obtained as $\bar{\bar{I}}_G = \sum_i \bar{\bar{I}}_{Gi}$.

Hydrodynamic Forces.

For a given fluid velocity field, the strain-rate tensor is defined as, $\bar{\bar{E}} = (\nabla \vec{v} + (\nabla \vec{v})^T)/2$, where T is the transpose and $\vec{\Omega} = \nabla \times \vec{v}/2$ is the angular velocity of the fluid. The operators ∇ and $\nabla \times$ denote the gradient and the curl, respectively. The characteristic shear rate of the flow for segment i is given as $\dot{\gamma}_i = \sqrt{(\bar{\bar{E}}_i : \bar{\bar{E}}_i)/2}$, where $\bar{\bar{E}}_i = \bar{\bar{E}}(\vec{r}_i)$ and : is the double inner product. The characteristic shear rate for the fiber is then computed as $\dot{\gamma} = \sum_{i=1}^N \dot{\gamma}_i / N$. The segment Reynolds number is defined as $\mathrm{Re}_s = \rho d \Delta v / \eta$, where ρ is the density of the fluid, η is its dynamic viscosity, d is the fiber diameter and Δv is the characteristic velocity difference between the fibers and the fluid. Here, we choose $\Delta v = L \dot{\gamma}$, where L is the fiber length . The hydrodynamic forces are dominated by viscous effects at small segment Reynolds numbers $\mathrm{Re}_s \ll 1$, and by inertia effects for large segment Reynolds numbers $\mathrm{Re}_s \gg 1$. Lindström and Uesaka (2007) numerically investigated the consequence of expressing viscous and inertia drag as a sum of two separable components, and found a fair agreement between the model, theory and experiments for a cylinder in cross-flow in the viscous flow regime, $\mathrm{Re}_s \leq 10^{-1}$, as well as in the regime dominated by dynamic effects, $10^2 \leq \mathrm{Re}_s \leq 3 \times 10^5$. The maximum error in drag coefficient C_D is 42% , found in the intermediate interval of Reynolds numbers at $\mathrm{Re}_s \approx 5.4$ (Re_s was based on the cross-flow velocity in those numerical experiments) . The total force and torque exerted on fiber segment i by the fluid are then given by

$$\vec{F}_i^h = \vec{F}_i^{h,v} + \vec{F}_i^{h,I} \tag{6}$$

$$\vec{T}_i^h = \vec{T}_i^{h,v} + \vec{T}_i^{h,I} \tag{7}$$

The viscous drag force of a fiber segment is here approximated with that of a prolate spheroid. An analytical solution described by Kim and Karilla (1991) is available for the viscous drag force on an isolated spheroidal particle under creeping flow conditions. According to the semi-empirical formula of Cox (1971), a prolate spheroid is hydrodynamically equivalent to a finite circular cylinder in the sense that their orbiting behavior in shear flow is the same if

$$\frac{r_e}{r_c} = 1.24 \frac{1}{\sqrt{\ln(r_c)}}, \tag{8}$$

where r_e is the so-called equivalent aspect ratio of the

prolate spheroid and r_c is the cylinder aspect ratio. For fiber segment i with aspect ratio $r_c = l_i/d_i$, we choose the major axis of the hydrodynamically equivalent prolate spheroid to be $a_i = l_i$. Its minor axis, b_i is then obtained by inserting $r_e = a_i/b_i$ into Cox's formula, becoming

$$b_i = \frac{1}{1.24} d_i \sqrt{\ln \frac{l_i}{d_i}}. \qquad (9)$$

Cox's formula is valid for isolated particles and a slender-body approximation. None of these assumptions are true for fiber segments. However, Lindström and Uesaka (2007) performed numerical experiments, which have shown that the error in the model predictions of the orbit period of rigid fibers in shear flow is less than 3.4% compared to Eq. (7) for $r_c \geq 10$ when a two-way coupling is considered. The viscous hydrodynamic force $\vec{F}_i^{h,v}$ and torque $\vec{T}_i^{h,v}$ are then estimated by

$$\vec{F}_i^{h,v} = \overline{\overline{A}}_i^{v} \cdot (\vec{v}(\vec{r}_i) - \dot{\vec{r}}_i) \qquad (10)$$

$$\vec{T}_i^{h,v} = \overline{\overline{C}}_i^{v} \cdot (\vec{\Omega}(\vec{r}_i) - \vec{\omega}_i) + \overline{\overline{\overline{H}}}_i^{v} : \overline{\overline{E}}(\vec{r}_i). \qquad (11)$$

The hydrodynamic resistance tensors $\overline{\overline{A}}_i^{v}$, $\overline{\overline{C}}_i^{v}$ and $\overline{\overline{\overline{H}}}_i^{v}$ are defined by Kim and Karilla (1991).

In the range $10^2 \leq Re_s \lesssim 3 \times 10^5$ of segment Reynolds numbers, the inertia drag force of a cylinder in cross-flow is dominant as compared to the viscous drag in the axial or cross-direction. If $\hat{z}_i$ is the cylinder orientation, then only the flow components in the plane perpendicular to $\hat{z}_i$ need to be considered. The drag coefficient for cross flow over a circular cylinder is, according to Tritton (1988), $C_D^I = 1.0$, for $10^2 \leq Re_s \lesssim 3 \times 10^5$. The total drag force and torque on a cylindrical fiber segment are obtained through integration over the infinitesimal cylinder slices. The dynamic drag force and torque are then given by

$$\vec{F}_i^{h,I} \approx \overline{\overline{A}}_i^{I} \cdot (\vec{v}(\vec{r}_i) - \dot{\vec{r}}_i) \qquad (12)$$

$$\vec{T}_i^{h,I} \approx \overline{\overline{C}}_i^{I} \cdot (\vec{\Omega}(\vec{r}_i) - \vec{\omega}_i) + \overline{\overline{\overline{H}}}_i^{I} : \overline{\overline{E}}(\vec{r}_i), \qquad (13)$$

where the dynamic drag resistance tensors are derived by Lindström and Uesaka (2007). The fluid velocity $\vec{v}(\vec{r}_i)$ is directly interpolated from the flow field.

Discretized Fiber Equations of Motion.
The fiber equations of motion are discretized in time with a time step Δt. Subscripts $n-1$ and n denote the previous and the current time step, respectively. An implicit numerical scheme is used for calculating the segment velocity and angular velocity to enhance numerical stability. Using the expression for the hydrodynamic force, Eq. (1) can be discretized as

$$\frac{m}{\Delta t}(\dot{\vec{r}}_{G,n} - \dot{\vec{r}}_{G,n-1}) = \sum_i \{(\overline{\overline{A}}_{i,n-1}^{v} + \overline{\overline{A}}_{i,n-1}^{I}) \cdot (\vec{v}(\vec{r}_{i,n-1}) - \dot{\vec{r}}_{i,n}) + \vec{F}_i^{w}\} \qquad (14)$$

where $\dot{\vec{r}}_{i,n} = \dot{\vec{r}}_{G,n} + \vec{\omega}_n \times \vec{r}_{Gi,n-1}$.

Using the expression for the hydrodynamic force and torque, Eq. (2) can be discretized as

$$\overline{\overline{I}}_{G,n-1} \cdot \frac{\vec{\omega}_n - \vec{\omega}_{n-1}}{\Delta t} + \vec{\omega}_n \times (\overline{\overline{I}}_{G,n-1} \cdot \vec{\omega}_{n-1}) =$$
$$\sum_i \{(\overline{\overline{C}}_{i,n-1}^{v} + \overline{\overline{C}}_{i,n-1}^{I}) \cdot (\vec{\Omega}(\vec{r}_{i,n-1}) - \vec{\omega}_n)$$
$$+ (\overline{\overline{\overline{H}}}_{i,n-1}^{v} + \overline{\overline{\overline{H}}}_{i,n-1}^{I}) : \overline{\overline{E}}(\vec{r}_{i,n-1})$$
$$+ \vec{r}_{Gi,n-1} \times ((\overline{\overline{A}}_{i,n-1}^{v} + \overline{\overline{A}}_{i,n-1}^{I}) \cdot (\vec{v}(\vec{r}_{i,n-1}) - \dot{\vec{r}}_{i,n}) + \vec{F}_i^{w})\}. \qquad (15)$$

The discretized equations are solved for $\dot{\vec{r}}_{G,n}$ and $\vec{\omega}_n$, from which the linear velocities $\dot{\vec{r}}_{i,n}$ of the segments are computed. The new segment positions and orientations become

$$\vec{r}_{i,n} = \vec{r}_{i,n-1} + \Delta t \dot{\vec{r}}_{i,n} \qquad (16)$$

$$\hat{z}_{i,n} = \hat{z}_{i,n-1} + \Delta t (\vec{\omega}_n \times \hat{z}_{i,n-1}). \qquad (17)$$

A correction of the segment positions is done at each time step to preclude the accumulation of errors. As in the algorithm implemented by Lindström and Uesaka (2007), the middle fiber segment is fixed in space and all the other segments are translated to maintain the exact original fiber length.

Random Walk Model.
The flow calculations do not resolve the smallest turbulent eddies. It is thus necessary to construct a representation of the fluctuating flow field that is superimposed on the mean flow field. Such a stochastic model of the flow fluctuations was proposed by Gosman and Ioannides (1983). The model consists of adding the local fluctuating component to the fluid velocity at the segment position, i.e. $\vec{v}(\vec{r}_i)$ becomes

$$\tilde{\vec{v}}(r_i) = \vec{v}(\vec{r}_i) + \vec{v}^{fluct}(\vec{r}_i) \text{ (Gosman and Ioannides 1983)}.$$

The local fluctuating component is estimated as

$$\vec{v}^{fluct}(\vec{r}_i) = \vec{\psi} \sqrt{\frac{2}{3} k(\vec{r}_i)} \qquad (18)$$

where $\sqrt{2k(\vec{r}_i)/3}$ is the local root mean square (RMS) of the fluid velocity fluctuation for isotropic turbulence and

$\vec{\psi} = (\psi_1, \psi_2, \psi_3)$ is a vector whose components are random numbers generated from a Gaussian distribution of zero mean and variance one. A vector $\vec{\psi}$ is generated for each fiber at each time step. The eddy life-time t_i^e and the time needed by the segment to transverse the eddy , *i.e.* the transit time t_i^{tr}, are calculated as

$$t_i^e = \frac{l_i^e}{u_i^e} = \frac{C_\mu^{0.63} k^{3/2}(\vec{r}_i)/\varepsilon(\vec{r}_i)}{\left|\upsilon^{fluct}(\vec{r}_i)\right|} \qquad (19)$$

$$t_i^{tr} = -\tau_i \ln\left(1 - \frac{l_i^e}{\tau_i \left|\tilde{\vec{\upsilon}}(\vec{r}_i) - \vec{\upsilon}(\vec{r}_i)\right|}\right), \qquad (20)$$

where $\tau_i = m_i / 3\pi\eta l Y^A$ is a segment relaxation time, which is defined as the ratio between the segment mass and the prefactor of the viscous component of the hydrodynamic force. The interaction time is defined as $\Delta t_i^t = \min\left(t_i^e, t_i^{tr}\right)$ and $\Delta t^t = \min\left(\Delta t_i^t\right), i \in 1, N$. The velocity $\tilde{\upsilon}(r_i)$ is kept constant during the interaction time Δt^t to evaluate the hydrodynamic forces and torques acting on the fiber segments and thus the linear and angular velocity of the fiber's center of mass (see Eqs. 14-15).

Time Step Constraints. The time step constraint due to the relaxation time of fiber-fluid system is

$$\Delta t << m/\eta L, \qquad (21)$$

where L is the fiber length. The other constraint is that the segments cannot move more than a fraction of its diameter at each time-step, *i.e.*

$$\Delta t << 1/r_c\dot{\gamma}. \qquad (22)$$

Since the time step used to solve Eqs. (14) and (15) with the modified velocity $\tilde{\upsilon}(r_i)$ can be shorter than the interaction time, the time step used in the simulations is

$$\min(\Delta t, \Delta t_{turb}). \qquad (23)$$

Fiber Model Validation

The period of revolution of an isolated fiber in shear flow is validated against the theoretical result for Jeffery's orbits.

Isolated Fiber in Simple Shear Flow Jeffery (1922) studied the motion of isolated prolate spheroids in simple shear flow. He showed that a prolate spheroid with an aspect ratio r_s undergoes periodic motion, so-called Jeffery orbits,

and it spends most of the time aligned with the flow direction. The period of revolution is $T = 2\pi$ $(r_s + 1/r_s)/\dot{\gamma}$ and increases with r_s. Bretherton (1962) showed that any axisymmetric particle in a linear flow gradient rotates with a period $T = 2\pi (r_e + 1/r_e)/\dot{\gamma}$, where r_e is an equivalent aspect ration that depends on the particle shape. The equivalent aspect ratio for a circular cylinder is given by Eq. (8). We carried out the simulations of Jeffery's orbits for an isolated rigid fiber in a simple shear flow using the implemented model. The fiber has diameter d =20 μ m, length L =1 mm and density ρ =1380 kgm^{-3}, which are all consistent with the properties of the hardwood fibers that are used later in the applied fiber flow simulations. The computational domain is a box of side 0.01 m and it is discretized into a rectangular mesh with ten cells in each direction. The number of cells is chosen to accurately resolve the imposed flow gradient. The fluid properties are $\eta = 1.6$ Pas and $\dot{\gamma} = 200$ s^{-1}. We compare the simulated orbit period of the rigid fiber with the one computed using Jeffery's equation in conjunction with Cox's equation for the equivalent aspect ratio of a circular cylinder. The simulated orbit period is overestimated by 10%. This discrepancy is due to the simplifying assumption of a one-way coupling between the fiber and the fluid phase (Lindström and Uesaka 2007).

Flow Case for Application of the Fiber Model

The fiber model is applied to the swirling flow in a conical diffuser. The flow case, the boundary conditions and a validation of the resulting flow are presented.

Flow Case Description. The ERCOFTAC conical diffuser test case is a swirling boundary layer developing in a conical diffuser (Claussen *et al* 1993). The swirling flow is generated by a rotating cylinder with a honeycomb at the inlet. After the honeycomb the flow becomes a plug flow with a solid body rotation (swirl).

The computational set-up is built according to the experimental case and the flow simulations are carried out using the OpenFOAM open source CFD code under steady-state conditions (Nilsson *et al.* 2008). The computational domain and its view with the relevant cross-sections are shown in Figs. 2-3.
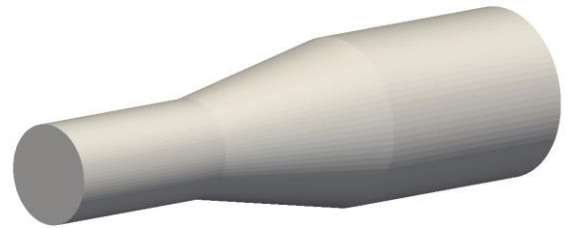

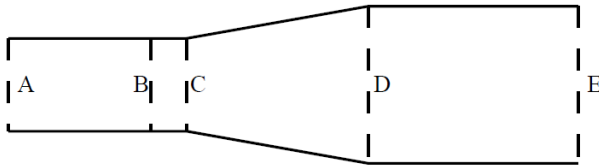**Figure 2:** ERCOFTAC conical diffuser geometry for the

computational test case.

Figure 3: A view of the ERCOFTAC conical diffuser.

Figure 4: ERCOFTAC conical diffuser – measurement traverses and their distance from the inlet of the conical region. (Nilsson *et al.* 2008).

The honeycomb is located at cross-section A. The cylindrical wall between A and B is rotating and the honeycomb is attached to this rotating cylinder, so that it also rotates. Cross-section C is the inlet of the expansion, D is the outlet of the expansion and E is the outlet of the artificial extension and the outlet of the computational domain. Section E-F was not present in the experimental set-up, *i.e.* the diffuser was open to the room. The geometrical parameters can be summarized as: the inlet diameter is 0.26 m, the diffuser length is 0.51m, the opening angle (for the conical region) is 10 deg and the extension length(D-E) is 0.59 m. The honeycomb has two purposes: first, to generate a plug flow and, secondly, to provide a well-defined vortex (solid-body). Thus, in the simulation, a plug flow is set in the axial direction according to the volume flow, and a tangential velocity is set according to solid-body rotation. Here, the axial velocity of the plug flow is U=11.6 ms^{-1} and the solid body rotation is Ω=52.646s^{-1}. The turbulence is specified using the turbulence length scale l_t = 0.0032m, corresponds to the size of the holes in the honeycomb, and the turbulence intensity I = 0.1, which is typically used in CFD. The ratio between the turbulent viscosity and the laminar viscosity is ν_t/ν =27.28.

The $k-\varepsilon$ model with wall functions is used to model the turbulence (Jones and Launder 1972) .The second-order upwind discretization scheme is used for the velocity, while the first-order upwind scheme is used for the turbulent quantities. (Versteeg and Malalasekera 1995).

Flow Validation. The flow results are validated using the experimental results of Clausen *et al* (1993). The measurements were done at several different traverses along the periphery of the diffusor, as depicted in Fig. 4. A comparison between simulations and experiments for the velocity profile and the turbulent kinetic energy profile is made at the traverses located 25 mm and 405 mm from position D. The comparison is shown in Figs.5-8. Here, U denotes the axial velocity component, W the tangential velocity component, U_0 is the bulk velocity at the inlet, and y is the wall normal distance. The validation shows that the computational results are in fair agreement with the experimental ones. Thus, the computed flow field is considered representative for studying the fiber motion.
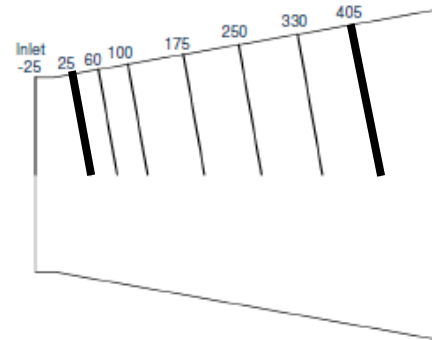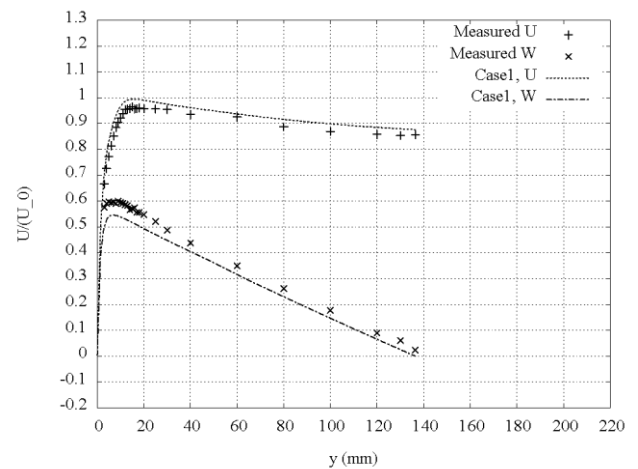

Figure 5: Comparison between the measured and computed axial (U) and tangential (W) velocities along the traverse 25 mm from position D.
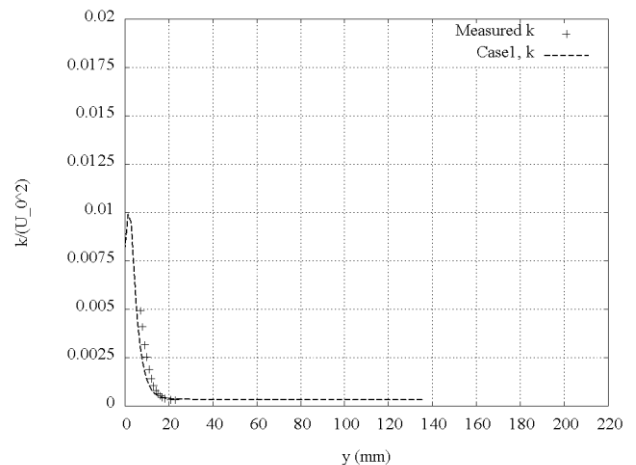

Figure 6: Comparison between the measured and computed turbulent kinetic energy along the traverse 25 mm from position D.
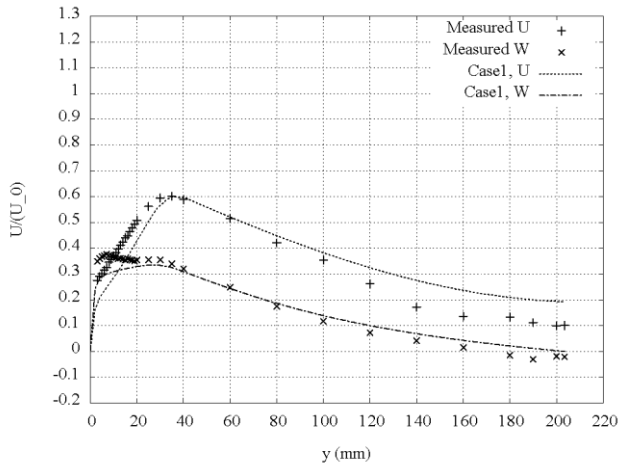
Figure 7: Comparison between the measured and computed axial (U) and tangential (W) velocities along the traverse 405 mm from position D.

Figure 8: Fibers at their initial positions at the inlet of the computational domain. The fiber diameters are exaggerated for the purpose of visualization.
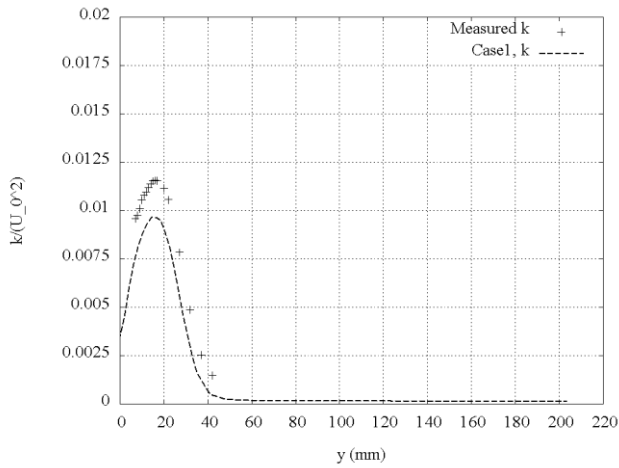

Figure 8: Comparison between the measured and computed turbulent kinetic energy along the traverse 405mm from position D.

Fiber Flow Results

The reorientation of the fibers due to the turbulent flow is studied, for different initial positions and concentrations.

Fibers in the ERCOFTAC case. The steady-state flow result for the ERCOFTAC case is used for simulating the fiber motion. Four cases are studied, in which the segments' length and density are varied. For the base case the segment diameter is $d = 20 \mu$ m, the segment length is $l = 0.2$ mm and the segment density is $\rho = 1380$ kgm^{-3} (all consistent with a hardwood fiber). In the following , we take these to be the fiber properties unless they are specified differently. In each case a total of 50 vertical fibers are placed at the inlet of the computational domain (see Fig.8). Each fiber consists of five segments. Neither the fiber-fiber nor the fiber-wall interactions are taken into account. A one-way coupling between the fiber and the fluid is considered, and the random walk model is used for the turbulent fluctuation. The trajectories of the flowing fibers are integrated for the full length of the diffusor.
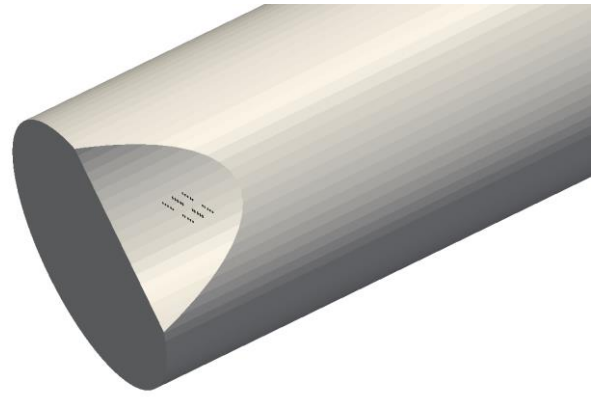
Fiber Reorientation. All the segments within one fiber have the same orientation, which is the orientation of the fiber. We define the allignment of the fiber with the flow directon as $z_3 = \hat{z} \cdot \hat{e}_3$, $-1 \leq z_3 \leq 1$ and use $|z_3|$ to quantify the orientation. We consider the development of the enemble average of $|z_3|$. The orientation exhibits an initial ramp, whose characteristic time scale is ~0.1 s (see Fig. 9). This time scale is in the order of inverse shear rate, as predicted for fibers in a linear shear gradient (Jeffery 1922). This implies that the alignment of fibers is mainly due to the average shear gradient, while the velocity fluctuations in the diffusor has a minor influence. In addition we show that introducing the random walk model does not influence the fiber reorientation (see Fig 9).
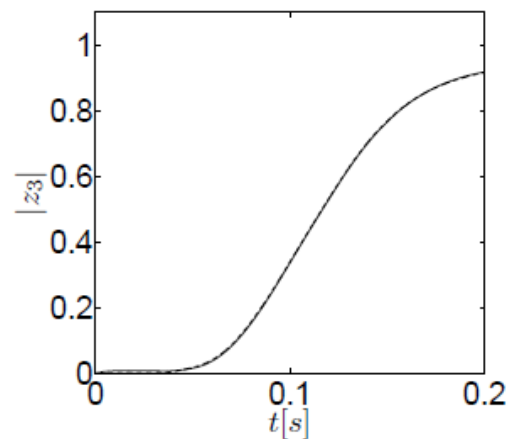

Figure 9: Alignment of initially vertical fibers. Ensemble average of $|z_3|$. Solid line: results with the random walk model; dashed line: results without the random walk model.

The influence icf fiber properties, such as segment length and segment density, on their reorientation is also analyzed. Simulations were conducted for two different species of fibers: one set with density ρ and the other with density

5ρ The orientation change in the initial phase is slower for the heavier fibers. The relaxation time of heavier fibers is longer, and thus, the initial ramp depends on fiber inertia (see Fig.10). When the segment length is varied between $l/2$ and $2l$ no significant effect on fiber motion is observed (Fig 11).
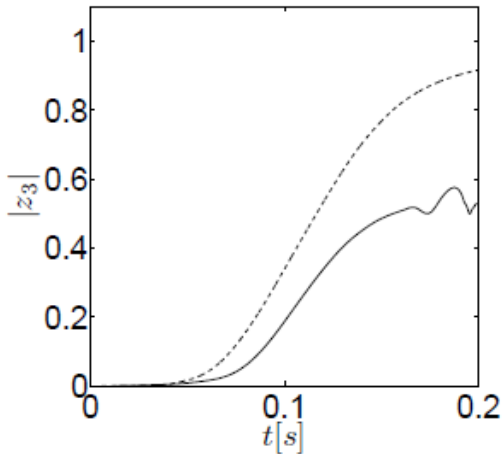

Figure 10: Alignment of initially vertical fibers– dependence on fiber density. Thin line: lower segment density; thick line: higher segment density.
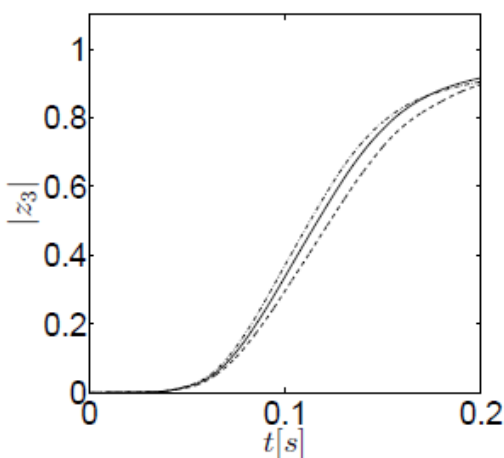
.

Figure 11: Alignment of initially vertical fibers – dependence on segment length. Solid line: segment length l; dashed line: segment length $l/2$; dashed-dotted line: segment length $2l$.

Conclusions

A particle-level rigid fiber model was integrated into a general purpose CFD code. The fibers are modeled as chains of rigid cylindrical segments and their parameters are typical for the hardwood fibers. The model was validated against the known analytical result for isolated fiber motion in linear shear gradient. The reorientation of the hardwood fibers suspended in the turbulent air-flow in a conical

diffuser was studied using the implemented model. The fluid flow is described using the incompressible Navier-Stokes equations with $k-\varepsilon$ turbulence model. It was found that the reorientation occurs at time-scale of the inverse average shear rate for the fibers and that the fiber inertia has a sinificant effect on the fiber reorientation, while the sensitivity to the fiber length at a constant fiber density is minor.

References

J. Andrić. Implementation of a flexible fiber model in a general-purpose CFD code. Thesis for Licentiate of Engineering no. 2012:04, Chalmers University of Technology, Göteborg, Sweden, 2012.

F.P. Bretherton. The motion of rigid particles in a shear flow at low Reynolds number, J. Fluid Mech. 14, 284–304 , 1962.

R. G. Cox. The motion of long slender bodies in a viscous fluid. Part 2. Shear flow. J. Fluid Mech., 45:625–657, 1971

P.D. Clausen, S.G. Koh and D.H. Wood. Measurements of a swirling turbulent boundary layer developing in a conical diffuser. Experimental Thermal and fluid Science, 6:39–48, 1993.
C. T. Crowe, M. Sommerfeld, and Y. Tsuji. Multiphase Flows With Droplets and Particles. CRC, New York, 1998.

O. L. Forgacs and S. G. Mason. Particle motions in sheared suspensions. IX. Spin and deformation of threadlike particles. J. Colloid Sci., 14:457–472, 1959a.

O. L. Forgacs and S. G. Mason. Particle motions in sheared suspensions. X. Orbits of flexible threadlike particles. J. Colloid Sci., 14:473–491, 1959b.

A.D. Gosman and E..Ioannides. Aspects of computer simulation of liquid-fueled combustors. Journal of Energy,7 :482-490, 1983.

J. Hämäläinen, S. B. Lindström, T. Hämäläinen, and T. Niskanen. Papermaking fiber suspension flow simulations at multiple scales. J. Eng. Math., 71(1):55–79, 2011.

G. B. Jeffery. The motion of ellipsoidal particles immersed in a viscous fluid. Proc. Roy. Soc. London Ser. A, 102:161–179, 1922.

W.P. Jones and B.E. Launder. The Prediction of Laminarization with a Two-Equation Model of Turbulence, International Journal of Heat and Mass Transfer, Vol.15, pp. 301–314, 1972.

S. Kim and S.J. Karilla. Microhydrodynamics: Principles and Selected Applications. Butterworth–Heinemann, Stoneham, 1991.

S. B. Lindström. Modeling and simulation of paper structure development. PhD thesis, Mid Sweden University, Sundsvall, Sweden, October 2008.

T. Matsuoka and S. Yamamoto. Dynamic simulation of fiber suspensions in shear flow. J. Chem. Phys., 102:2254–2260, 1995.

H. Nilsson, M. Page, M. Beaudoin, B. Gschaider, H. Jasak. The OpenFOAM turbomachinery working group, and conclusions from the turbomachinery session of the third OpenFOAM workshop. 24th Symposium on Hydraulic Machinery and Systems.Foz do Iguassu,October 27-31,2008.

D. Qi. Direct simulations of flexible cylindrical fiber suspensions in finite Reynolds number flows. J. Chem. Phys., 125:114901, 2006.

R. F. Ross and D. J. Klingenberg. Dynamic simulation of flexible fibers composed of linked rigid bodies. J. Chem. Phys., 106:2949–2960, 1997.

A. Salahuddin, J.Wu, and C. K. Aidun. Numerical study of rotational diffusion in sheared semidilute fiber suspension. J. Fluid Mech., 692:153–182, 2012.

C. F. Schmid, L. H. Switzer, and D. J. Klingenberg. Simulation of fiber flocculation: Effects of fiber properties and interfiber friction. J. Rheol., 44:781–809, 2000.

E.Svenning, A. Mark, F. Edelvik, E. Glatt, S. Rief, A. Wiegmann, L. Martinsson, R. Lai, M. Fredlund, and U. Nyman. Multiphase simulation of fiber suspension flows using immersed boundary methods. Nordic Pulp Paper Res. J., 27(2):184–191, 2012.

D. J. Tritton. Physical fluid dynamics. Clarendon, Oxford,1988.

H.K Versteeg and W. Malalasekera. An introduction to computational fluid dynamics. Pearson Education Limited, 1995.
H.G. Weller, G. Tabor, H. Jasak, and C.Fureby. A tensorial approach to computational continuum mechanics using object-oriented techniques. Comput. Phys., 12(6): 620–631, 1998.